Ceramics International 47 (2021) 22604–22614

Contents lists available at ScienceDirect

Ceramics International

journal homepage: www.elsevier.com/locate/ceramint

Increasing the photocatalytic and fungicide activities of Ag_3PO_4 microcrystals under visible-light irradiation

Lucas Portela Oliveira [a], Camila Cristina de Foggi [b,c,*], Bruna Natália Alves da Silva Pimentel [a], Marcelo Assis [b], Juan Andrés [c,**], Elson Longo [b], Carlos Eduardo Vergani [a]

[a] São Paulo State University (UNESP), School of Dentistry, Department of Dental Materials and Prosthodontics, 1680 Humaitá Street, Araraquara, São Paulo, 14801-903, Brazil

[b] Federal University of São Carlos (UFSCar), Department of Chemistry, 676 Washington Luis Highway, São Carlos, São Paulo, 13565-905, Brazil

[c] Universitat Jaume I (UJI), Department of Physical and Analytical Chemistry, Castellón de la Plana, 12071, Spain

ARTICLE INFO

Keywords:
Ag_3PO_4
Visible light
Photocatalysis
Rhodamine B degradation
Fungicide activity

ABSTRACT

The present study reports for the first time the performance of silver phosphate (Ag_3PO_4) microcrystals as photocatalyst (degradation of Rodamine B-RhB) and antifungal agent (against *Candida albicans–C. albicans*) under visible-light irradiation (455 nm). Ag_3PO_4 microcrystals were synthesized by a simple co-precipitation (CP) method at room temperature. The structural and electronic properties of the as-synthetized Ag_3PO_4 have been investigated before and after 4 cycles of RhB degradation under visible light using X-ray diffraction (XRD), micro-Raman spectroscopy, UV–Vis spectrophotometer and field emission scanning electron microscopy (FE-SEM) images. The antifungal activity was analyzed in planktonic cells and 48h-biofilm of *C. albicans* by colony forming units (CFU) counting, confocal laser and FE-SE microscopies. Statistical analysis was carried out using SPSS software. Morphological and structural modifications of Ag_3PO_4 were observed upon recycling. After 4 recycles, the material maintained its photodegradation property; an eightfold increase in the efficiency of Ag_3PO_4 was observed in planktonic cells and a two fold increase in biofilm when irradiated under visible light. Thus, higher antifungal effectiveness against *C. albicans* was obtained when associated with visible-light irradiation.

1. Introduction

Ag_3PO_4 microcrystals have excellent optical properties; photoluminescent, photocatalytic, bacteriostatic activity; and biocompatibility [1–12], which are important characteristics for materials used in the biomedical field. Moreover, Ag_3PO_4 microcrystals have photodegradation potential when exposed to light spectra. In addition, compared to organic photosensitizers, Ag_3PO_4 presents advantageous due to their greater stability under different biological conditions, such as pH, ionic strength, pressure, and stability to light [13,14].

C. albicans is a commensal fungus that lives in harmony with other microorganisms, but local or systemic factors (HIV, cancer, malnutrition, diabetes, chemotherapy, or radiotherapy) can alter this balance and promote *C. albicans* pathogenicity [15,16]. Denture stomatitis, for example, affects a large number of people using removable oral prostheses. It exhibits multifactorial etiology, including a higher incidence in women and smokers, inadequate prosthesis use, and microbial colonization, mainly by *Candida* spp [17], and especially by *C. albicans* [18]. The treatment currently used consists of antifungals such as miconazole [19], nystatin, or fluconazole. However, the infection caused by *C. albicans* presents frequent recurrence due to its multifactorial etiology and the lack of antifungal drug efficacy [20].

Among the possibilities for microbial control, the use of microcrystals of semiconductors composed of silver (Ag) has been widely investigated by our research group due to its high activity against bacteria, fungi, and viruses [21–27]. The great advantage of using microcrystals is the non-penetrability in mammalian cells, such as fibroblasts and keratinocytes, due to their larger dimensions [21,28,29], which increase biocompatibility.

Ag_3PO_4 exhibits photocatalytic activity in the presence of light [11], especially UV light because it presents greater light absorption. For the first time, in the present study, we investigate Ag_3PO_4 microcrystals as

* Corresponding author. Universitat Jaume I (UJI), Departament of Physical and Analytical Chemistry, Av. Vicent Sos Baynat, s/n, 12071, Castellón de la Plana, Spain.

** Corresponding author.

E-mail address: camilafoggi@gmail.com (C.C. Foggi).

https://doi.org/10.1016/j.ceramint.2021.04.272

Received 9 March 2021; Received in revised form 19 April 2021; Accepted 27 April 2021

Available online 3 May 2021

photocatalyst for the degradation of Rhodamine B (RhB) and as biocide against *C. albicans*, in the absence and presence of irradiation in the visible light range (blue) called L- and L+, respectively. This wavelength range was selected because it is commonly employed for the treatment of skin tumors [30], the analysis of melanoma growth rate [31], the treatment of colorectal cancer by the production of reactive oxygen species (ROS) [32], and in dentistry for chemical activation by light-curing of resin-based restorative materials [33,34].

Thus, the aim of this study was to evaluate the photocatalytic and antifungal activity of Ag_3PO_4 microcrystals against *C. albicans* and the effect of the presence or absence of visible-light irradiation.

2. Results and discussion

2.1. Characterization aspects

The analysis of the Ag_3PO_4 absorption spectrum (Fig. S1, in the Supporting Information) displays a maximum absorbance value of 1.493 a.u. at the wavelength of 325 nm. Although the absorption peaks in the ultraviolet wavelength (harmful to health) [35–37], the particles were also stimulated by blue light, with an absorbance of 1.252 a.u. at the 455-nm wavelength, because the photon energy from the light used is larger than the value of Egap for Ag_3PO_4 (2.24 eV) (Fig. S2). Besides, the 455 nm wavelength used in this research is already used in dental treatments; thus this is an area of interest for our research group for future development of the prevention or treatment of *C. albicans*-related diseases in the oral cavity. Thus, the light used in dental offices covers the visible spectrum of visible light at a specific wavelength of the blue region [38]. Fig. 1 shows the photocatalytic activity of Ag_3PO_4 against RhB upon four exposures to blue light (455 nm). RhB shows maximum absorbance between 500- and 600-nm wavelengths, and the degradation of the RhB chromophore was analyzed through the decay of this absorbance. This decay occurs due to the de-ethylation of the *N*, *N*′-diethylammonium group in the xanthene ring (chromophore of the RhB) [39]. From the first to the third cycle, there was an increase in the degradation rate of the RhB. In the fourth cycle, the degradation rated decreased. This result can be attributed to the structural and electronic modifications that the material undergoes in the photocorrosion processes for the degradation of the RhB.

The photodegradation results for 455 nm irradiation are shown in Fig. 2A. The RhB concentration (C_n/C_0) is presented as function of time, where C_n is the concentration at time t and C_0 is the initial concentration. Due to the low concentration of dye and catalyst in the tests, most heterogeneous photocatalytic mechanisms performed by semiconductors are considered pseudo-first-order [40]. Complete photodegradation of RhB after 30 min under visible-light irradiation was reported previously, with Ag_3PO_4 synthesized by a facile ion-exchange route [41]. In our study, after 12 min under visible-light irradiation, almost complete photocatalysis is observed in the first and third cycles. This RhB photodegradation time is in agreement with results reported in the literature with Ag_3PO_4 nanorods [42]. After 20 min, the rate of degradation was 100%, with the exception of the fourth cycle. The Ag_3PO_4 showed good photocatalytic performance under visible blue light irradiation even after 4 reuse cycles.

The Langmuir-Hinshelwood model (Fig. 2B) [43] was used to determine the photodegradation rate constant k (angular coefficient). As observed in Fig. 1, the k constants for the first and fourth cycle are 0.0834 and 0.0801 min^{-1}, respectively. They are lower because their degradation period is longer. In contrast, the speeds for the second and third cycles are higher, 0.1284 and 0.2223 min^{-1}, respectively. These results can be attributed to a synergistic effect between the semiconductor and the species generated during the RhB photodegradation process.

The morphological structure of a semiconductor is known to clearly

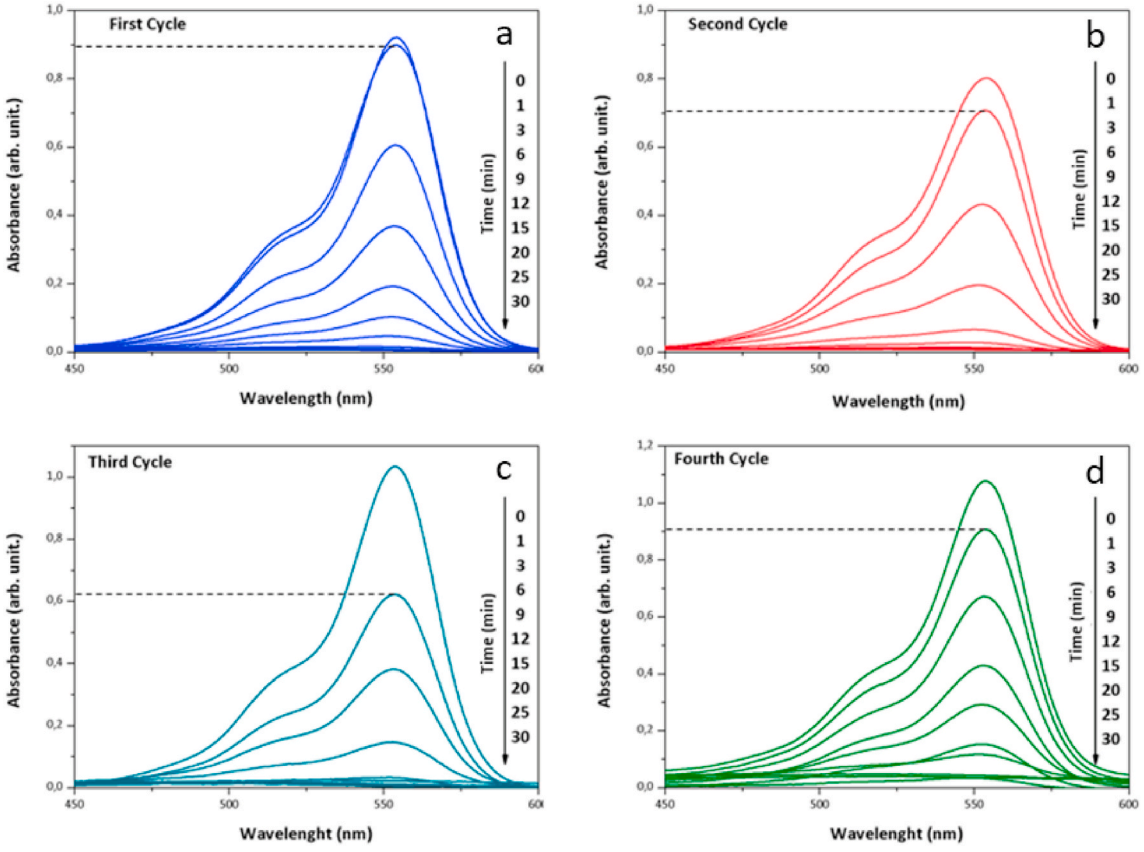

Fig. 1. Photocatalytic activity of Ag_3PO_4 after four exposures to visible light.

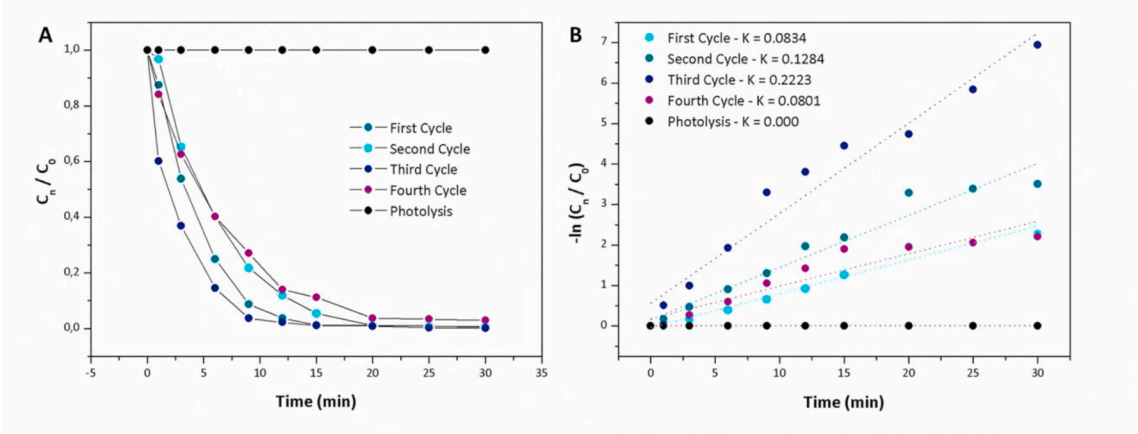

Fig. 2. Rhodamine degradation curve (a) and reaction kinetics (b).

affect photocatalytic performance, as photocatalytic reactions occur on its surface. Previous results of our research group point out that the incomplete local coordination of Ag cations at the exposed surfaces of the Ag_3PO_4 semiconductor are the active sites where the surface reactions, that include reduction by electrons, e^-, and oxidation by holes, h^+, take place [9].

To propose the mechanism of action of Ag_3PO_4 as a photocatalytic, reactive species trapping test was performed. As shown in Fig. S3, when BQ or AO were added to the system, there was a strong inhibition of the photodegradation process. When ISO was added, the photodegradation process occurred without significant changes.

Based on scavenger experiments a possible mechanism for the photocatalytic mechanism of RhB degradation is described as follows:

$$Ag_3PO_4 + h\nu \rightarrow h^+(\text{valence band}) + e^-(\text{conduction band}) \quad (1)$$

$$h^+ + H_2O \rightarrow \cdot OH + H^+ \quad (2)$$

$$e^- + O_2 \rightarrow \cdot O_2^- \quad (3)$$

$$\cdot O_2^- + \text{RhB} \rightarrow \text{degradation products} \quad (4)$$

The generation of reactive oxygen species occurs in the conduction and valence bands of the semiconductor. At the conduction band the e^- reacts with O_2 to render $\cdot O_2^-$ while h^+ reacts with H_2O to obtain $\cdot OH$. From the results of the scavenger experiments we can assume that the $\cdot O_2^-$ radical is responsible for degradation of RhB. The $\cdot OH$ radical does not participate directly in this process; however we cannot discard the presence of hydroxyperoxyl radical ($\cdot HO_2$). This radical can be obtained by the interaction between $\cdot O_2^-$ and H^+, formed in the reaction (2). In addition the singlet oxygen, $^1O_2$, can be obtained by means of oxidation: $\cdot O_2^- \rightarrow {}^1O_2 + e^-$.

XRD was performed to verify the order/disorder related to the crystallinity of Ag_3PO_4 at a long range. This technique identified parameter changes due to the light cycles, and it determined the phases formed in the pure material and the resulting cycles through the *Inorganic Crystal Structure Database* (ICSD). Fig. 3A shows that the pure material exhibits only the cubic phase of Ag_3PO_4, which is identified by the ICSD 14000 [44] with a cubic structure and belonging to the group *P*43*n* and the main peak (210) located at 33.2°. Moreover, it can be concluded that the material has a good crystallinity due to the sharp definition of the diffraction peaks. As the cycles are performed, cubic and hexagonal metallic Ag are formed. They belong to the space groups *Fm-3m* and *P*6$_3$*/mmc*, respectively, identified by ICSD 44387 [45] and ICSD 56269 [46], respectively. Cubic Ag already appears in the first cycle and becomes more intense until the fourth cycle, where there is more cubic Ag than Ag_3PO_4. The cubic Ag phase is characterized by the appearance of the diffraction planes (111), (200), (220), (311) and (222) located at 37.9, 44.5, 64.4, 77.3 and 81.3° respectively. In the third cycle, hexagonal Ag starts to appear, evidenced by the presence of the diffraction planes (110) and (201) located at 35.9 and 40.9° respectively. This behavior occurs due to the disassembly of the [AgO_4] cluster in Ag_3PO_4, which causes the Ag phase of higher stability (cubic) to be obtained first and become unstable (hexagonal) afterwards [47,48]. Moreover, a centralized amorphization halo was observed at 24°. They

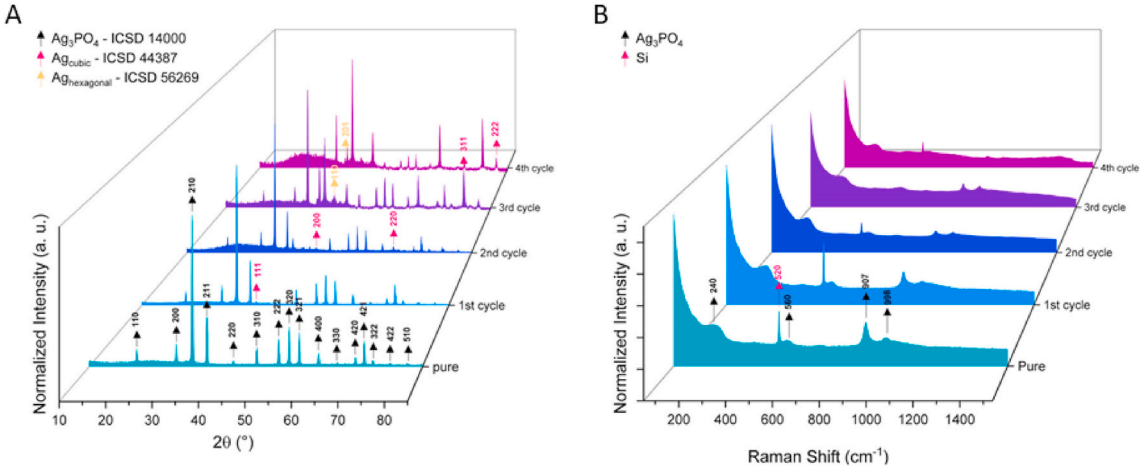

Fig. 3. (A) XRD patterns of Ag_3PO_4 after four exposures to visible light and (B) Micro-Raman spectroscopy of Ag_3PO_4 after four exposures to visible light.

increase proportionally to the number of cycles, demonstrating the low crystallinity of the system. This phenomenon occurs through the irradiation of the material, where in the [AgO_4] clusters the reduction process takes place, leading to the formation of metallic Ag. This process favors the decomposition of Ag_3PO_4, which leads to the formation of an amorphous material composed of $Ag_xP_yO_z$ and reduces the crystallinity of the final system.

When the formation of cubic Ag occurs during the photodegradation process, a heterostructure is formed, Ag_{cubic}/Ag_3PO_4. The synergistic effect between these two phases increases the RhB photodegradation rate in the second and third cycles, as shown in Figs. 1 and 2, respectively. In contact with electromagnetic radiation, the electrons of the Ag nanoparticles (Ag NPs) provoke the surface plasmon resonance effect. These plasmon oscillations promote the electronic transfer processes, increasing the efficiency of heterostructures for photocatalytic processes [49]. In the fourth cycle, the photocorrosion process causes hexagonal Ag to be formed together with Ag_{cubic}/Ag_3PO_4, also reducing the rate of degradation. Thus, the formation of this specific phase increases the electron-hole recombination (e^--$h^\bullet$) of the system, which makes the process less efficient than the previous ones.

Micro-Raman spectroscopy was performed to analyze order/disorder of the system at short range (Fig. 3B). According to the group theory, through the decomposition of the Γ point, Ag_3PO_4 has 18 active modes in the Raman, given by $2A_1 + 4E + 12T_2$. However, due to the high disorder at short range, only four modes were observed, at 240, 560, 907, and 998 cm^{-1}. The 240 cm^{-1} (T_2) mode is related to the characteristic rotation/translation of the [PO_4] cluster. The mode at 560 cm^{-1} (E) refers to the asymmetric bending of the [PO_4] cluster. The modes at 907 (A_1) and 998 cm^{-1} (T_2) refer to symmetrical and asymmetrical stretching, respectively, and the symmetrical stretching is more intense. As the material is recycled through photocatalysis, an increase of the short-range disorder occurs due to the dissipation of the modes mentioned above. This behavior can be attributed to the structural degradation of Ag_3PO_4 during the photocatalytic cycles, which favors the formation of secondary materials (cubic and hexagonal Ag, observed in the XRD). Thus, the characteristic modes of the matrix become less intense, due to the increase in the structural disorder of Ag_3PO_4.

Fig. 4 shows the FE-SEM micrographs for the pure Ag_3PO_4 and after the RhB photodegradation cycles. The characteristics of the photocatalysis depend on the morphology of the material. Based on the parameters used in the synthesis, such as temperature and surfactants, several morphologies can be obtained such as polyhedra, circles, and particles with irregular morphology. In this study, the CP method applied to the synthesis of Ag_3PO_4 presented a morphology of agglomerated irregular spheres (Fig. 4A and B). As the RhB photodegradation cycles were performed, degradation on the surfaces of these spheres was observed, as shown in Fig. 4C–J. This occurred due to the degradation of Ag_3PO_4 for the formation of metallic Ag, which was confirmed by XRD and Micro-Raman spectroscopy measurements. It was also observed that particle size decreases with increasing photocatalytic cycles, ranging from 294 ± 68 nm for the pure material to 107 ± 32 for the material obtained in the last cycle (for the first, second, and third cycles, 250 ± 51, 217 ± 53, and 142 ± 47 nm sizes were obtained, respectively). These results can be attributed to the degradation of Ag_3PO_4 in the photocatalytic process, which leads to the formation of other species, such as cubic and hexagonal Ag.

2.2. Antifungal activity of Ag_3PO_4 in the presence and absence of light

The antifungal activity of Ag_3PO_4 in different concentrations was evaluated against *C. albicans* ATCC 90028 in planktonic and biofilm in formation, in the presence (L+) and absence (L-) of visible-light irradiation (455 nm). A difference in inhibitory concentrations (IC) was observed between L+ and L-groups.

Two-way ANOVA showed that there is an interaction ($p < 0.001$) between the factors analyzed (light and concentration) on *C. albicans*, both in suspension and in biofilm formation. In *C. albicans* in suspension, two-way ANOVA showed that there is an effect of light [$F(1; 208) = 62.742$; $p < 0.001$], concentration [$F(12; 208) = 345.651$; $p < 0.001$], as well as the interaction between light and concentration [$F(12; 208) = 44.528$; $p < 0.001$] on the viability of *C. albicans*.

The suspension data was analyzed starting at 2000 μg/mL and decreasing to 0 μg/mL (control). Considering whether or not to use light at the same concentration of 125 or 62.5 μg/mL, the mean Log_{10} (CFU/mL) in the L+ were significantly higher than those in the L-. The results in the L-showed that CFU started to decrease at 62.5 μg/mL and decreased at higher concentrations of Ag_3PO_4. In L+, the mean CFU was significantly lower at 125 μg/mL compared to the remaining minor concentrations (≤23% of reduction). Although presenting a higher percentage of kill in sub-MFC in L- (concentration of 1000 μg/mL, with a reduction of 42%) compared to the sub-MFC in L+ (concentration of 125 μg/mL, with a reduction of 23%), there was a significant reduction in particle concentration required to completely eliminate microorganisms from 2000 to 250 μg/mL, suggesting the efficacy of a lower silver phosphate particle concentration for MFC in L+.

The inhibition of microorganism was total whenever light was present at 250 μg/mL or higher concentrations. However, in the absence of light, inhibition was only complete at the highest concentration of Ag_3PO_4 (2000 μg/mL).

In biofilm formation, two-way ANOVA also showed that there is an effect of visible light [$F(1; 96) = 43.121$; $p < 0.001$], and concentration [$F(5; 96) = 141.428$; $p < 0.001$], as well as the interaction between light and concentration [$F(5; 96) = 28.374$; $p < 0.001$] on the viability of *C. albicans* cells. The absence and presence of visible light and the microcrystal concentrations (0 μg/mL to 1000 μg/mL) were used as fixed factors. At 1000 μg/mL, the mean Log_{10} (CFU/mL) was

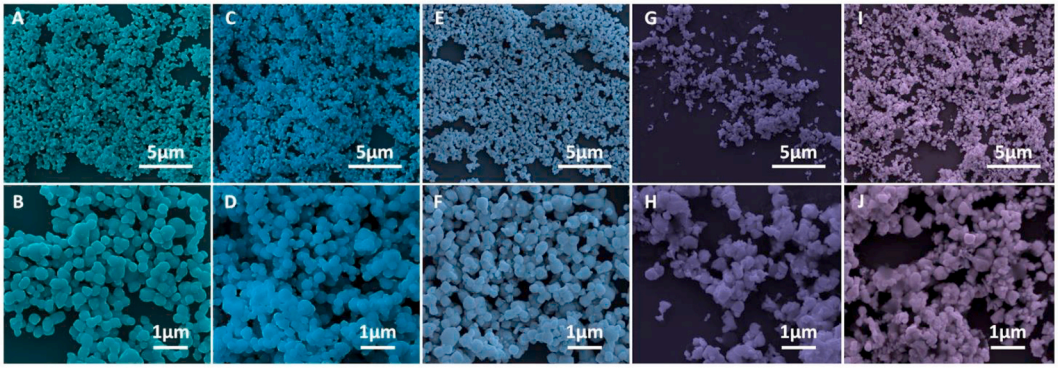

Fig. 4. FE-SEM of Ag_3PO_4 microcrystals on different magnifications. Pure (A), after one (C), two (E), three (G), and four (I) exposures to visible-light and the respective magnifications at B, D, F, H, and J.

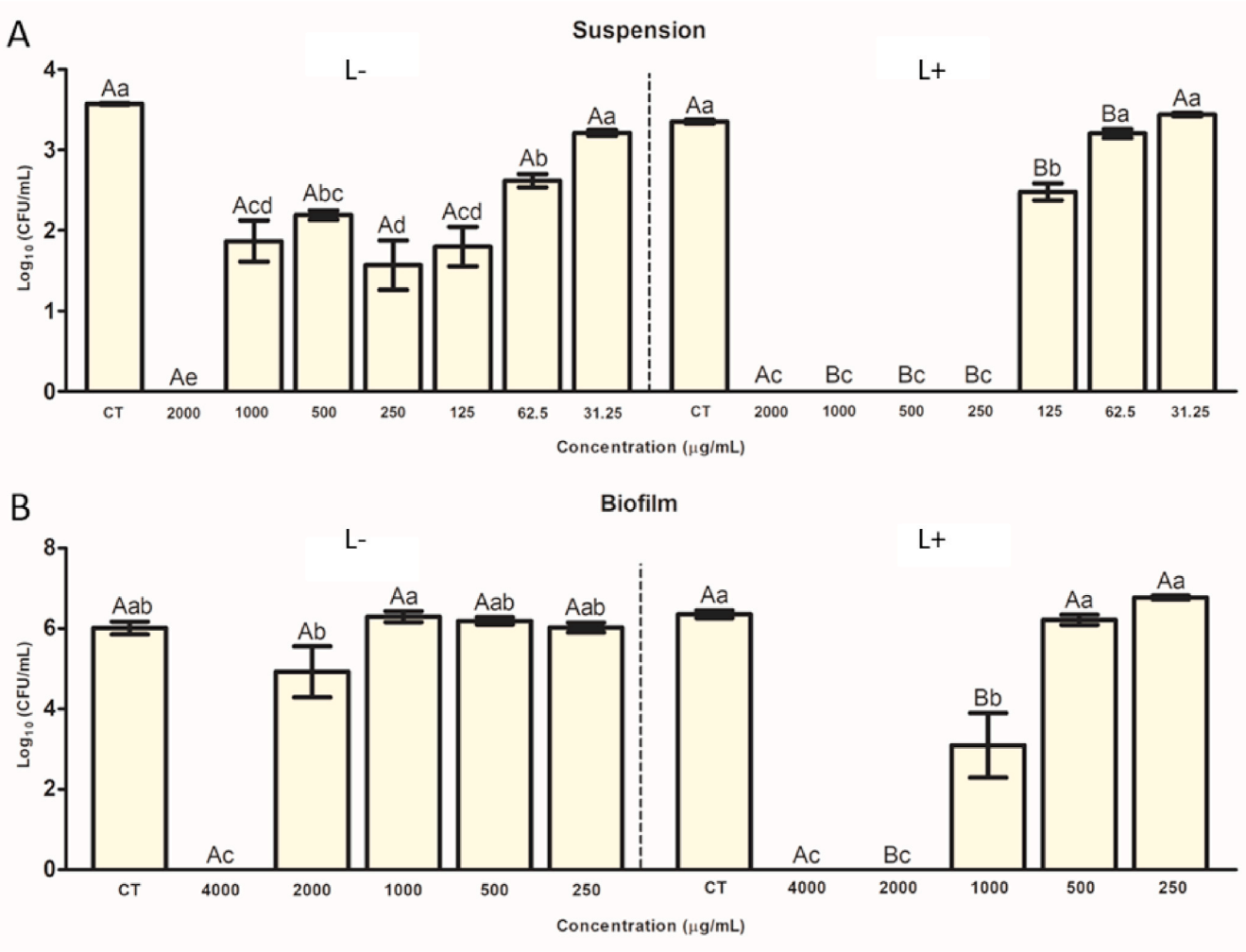

Fig. 5. Mean values of Log_{10}(CFU/mL) of *C. albicans* in suspension (A) and biofilm formation (B) after treatment with different concentrations of Ag_3PO_4 in the presence and absent visible-light irradiation. CT: control; L-: without visible-light irradiation; L+: presence of visible-light irradiation. Error bars: standard deviation. Equal lowercase letters denote equality of means within the group (L+ or L-); Equal uppercase letters denote equality of means in the same concentration between the groups.

significantly lower in L+ (reduction of 23%) than in L- (no reduction), and it was equivalent in other concentrations (Fig. 5). In L+, the CFU averages were equivalent at concentrations from 500 to 0 µg/mL. The mean was lower for 1000 µg/mL, and higher and equivalent for other concentrations.

The data presented by the biofilm showed the minimal biofilm inhibitory concentration (MBIC) at 4000 µg/mL (100% of reduction) in L-, and at 2000 µg/mL in L+. Both sub-MBIC, in L- (2000 µg/mL) and L+ (1000 µg/mL), showed reduction compared to the control (6,5 % and 23 %, respectively), but the presence of light suggested a greater efficacy using lower silver phosphate particle concentration.

This information is in agreement with FE-SEM images (Fig. 6). A reduction of *C. albicans* was observed when compared to the image control microorganisms without Ag_3PO_4. In the FE-SEM images (Fig. 6), we can also observe a reduction in the growth of *C. albicans*, however, with no elimination of fungus. Nevertheless, the morphology of the blastopores was modified from round to irregular (Fig. 6D and H).

An analysis of confocal microscopy (Fig. 7) shows that the red staining (propidium iodide) becomes more intense as the concentrations increase, and it is inversely proportional to the green staining (SYTO 9). Moreover, the control group demonstrated a cluster of living microorganisms, which progressively decreased in other concentrations. These other concentrations presented black spaces, which may be characteristic of microorganism reduction. These results are in accordance with the Log_{10} (CFU/mL) data, where the difference between the control group and IC is significant ($p < 0.001$).

The microcrystals agglutinated throughout the tests to evaluate the inhibitory activity of the Ag_3PO_4 microcrystals against *C. albicans* during its biofilm formation. Methodological optimizations were necessary, changing the culture medium from RPMI to YNB, to avoid this problem and to allow an appropriate distribution of concentrations. The literature is clear regarding the growth of microorganisms according to the culture medium used, that is, the culture medium affects the growth, adhesion, and development of biofilms [50]. According to the previously mentioned study, the growth of *C. albicans* biofilm is favored when the RPMI medium is used, supporting the growth of hyphae and extracellular matrix [51], which are characteristics of a well-established biofilm. In this study, we chose to perform the tests with the YNB medium since the material agglutinated when in contact with the RPMI medium. The use of the YNB culture medium can reduce the metabolic activity of *C. albicans* biofilm, resulting in a biofilm with less evident characteristics [51], such as fewer hyphae development. These characteristics can be seen in Fig. 7.

As the particles are irradiated, morphological changes take place on the surface of the material. These changes are responsible for the release of Ag ions, which can interact with the plasma membrane, DNA, and enzymatic processes of the microorganisms, leading to their death [52, 53]. In addition, the energy provided by the photons and the surface

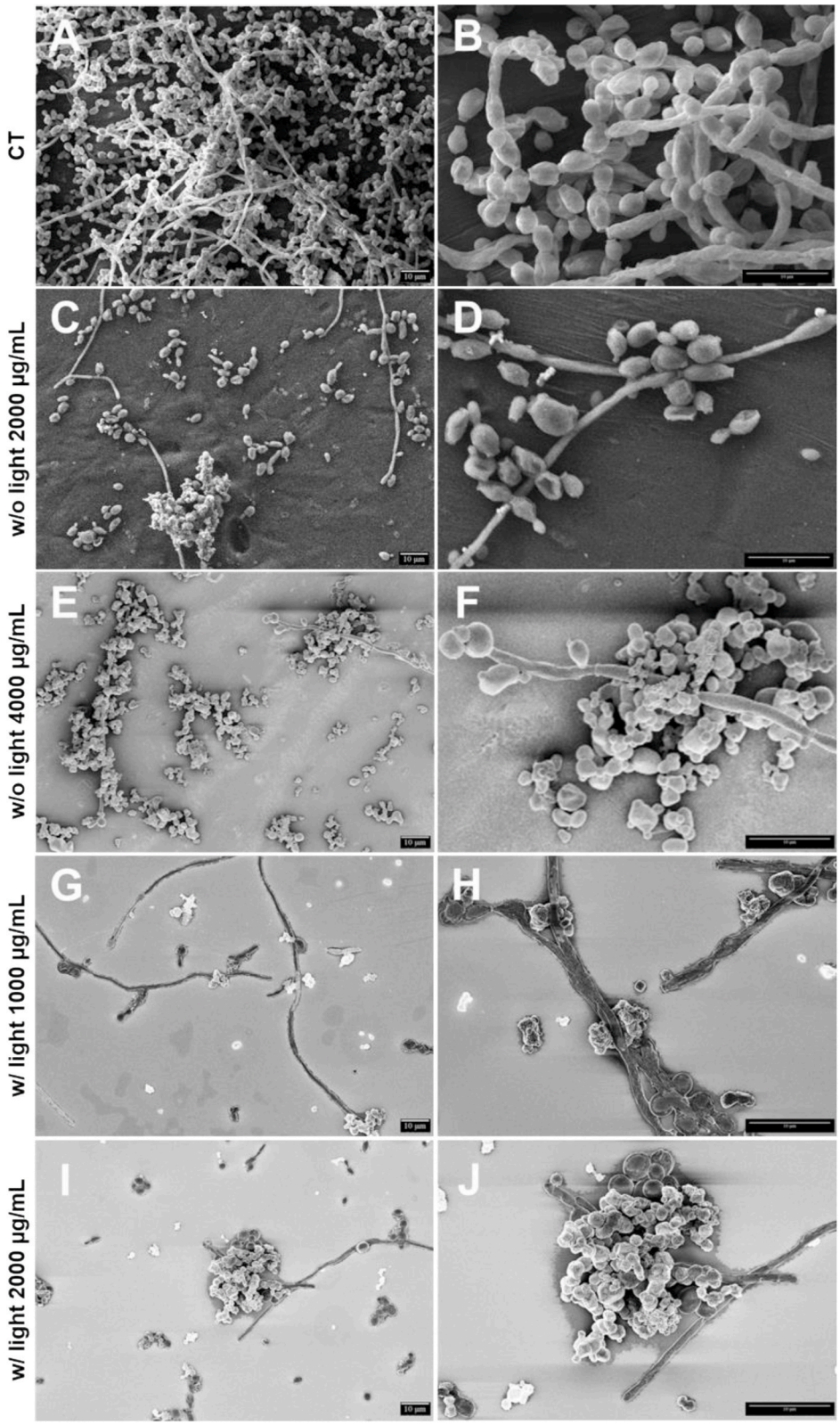

Fig. 6. FE-SEM of *C. albicans* biofilm formed in the presence of Ag_3PO_4 microcrystals without (w/o) and with visible-light irradiation (w/). The images (A) and (B) are control; (C–D) and (E–F) are 2000 µg/mL and 4000 µg/mL; (G–H) and (I–J), 1000 µg/mL and 2000 µg/mL. The (B), (D), (F), (H), (H) images are magnifications of (A), (C), (E), (G) and (I) images.

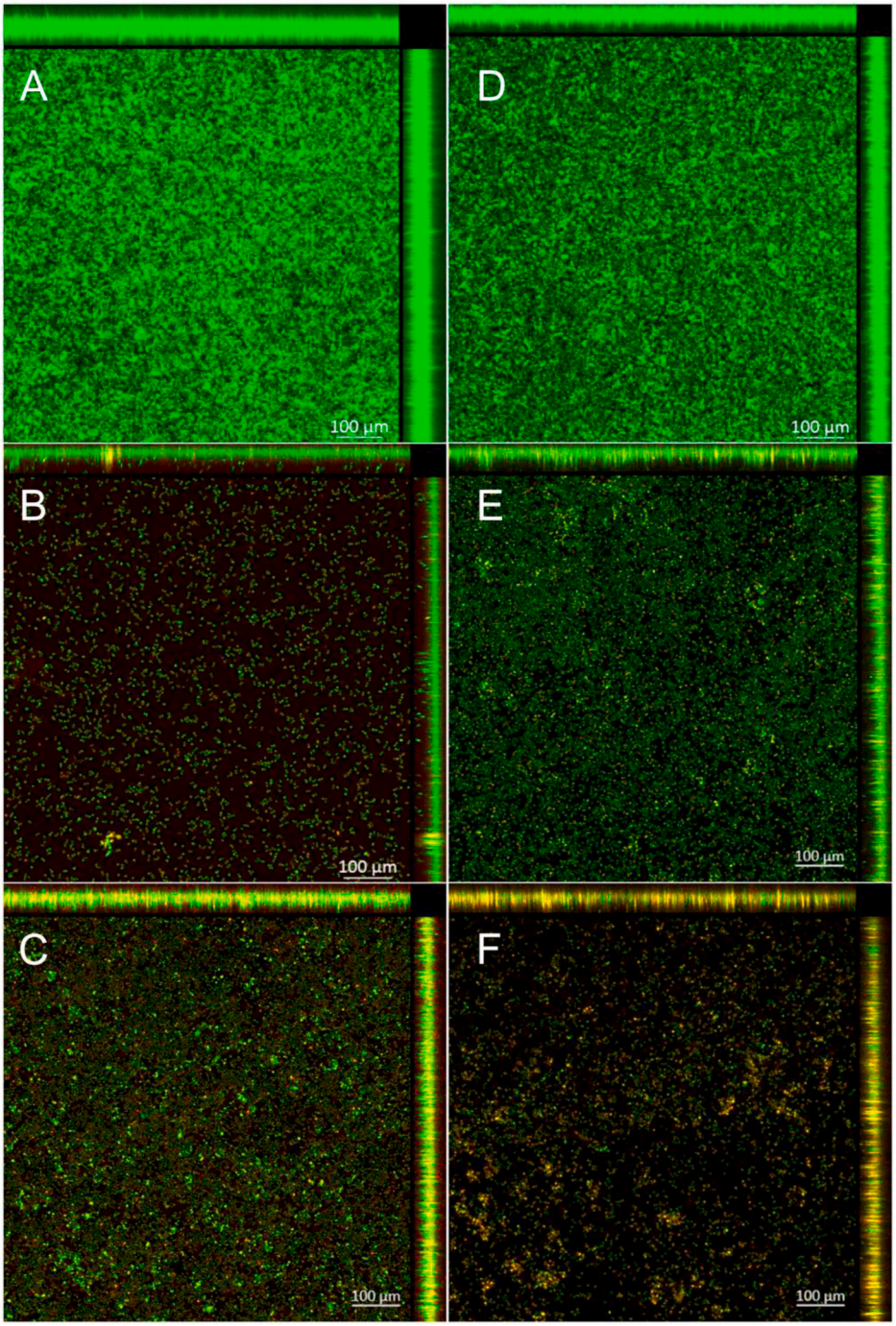

Fig. 7. Confocal microscopy of *C. albicans* biofilm formed in the presence of Ag_3PO_4 microcrystals with (A, B, C) and without visible-light irradiation (D, E, F). A and D represent the control group, followed by B and C (2000 and 4000 µg/mL), and E and F (1000 and 2000 µg/mL), with Ag_3PO_4 concentrations used against the biofilm.

plasmon resonance effect facilitates the migration of electrons. The main factor responsible for both RhB degradation and antifungal activity under visible-light irradiation is the same. It comes into contact with the cell wall and membrane, breaking them both. It also generates oxidative stress inside the cell, disrupting its intracellular structures, which can lead to cell death [54–56]. Moreover, ROS is generated inside the cells, possibly due to silver ions which inhibit the respiratory enzyme, which attacks itself [57]. Fig. 8 shows the schematic drawing of the mechanism of action of the Ag_3PO_4/Ag heterostructure when irradiated with blue light (455 nm).

Investigations were carried out to evaluate the growth rate of microorganisms in the presence of Ag_3PO_4 [58]. However, there are no studies in the literature regarding their action both against biofilm and in the presence of the fungus *C. albicans*, as analyzed in the present study. Compared to the suspension, the biofilm presented higher inhibitory and subinhibitory concentrations due to its greater complexity and the presence of an extracellular matrix, which is an inherent resistance of biofilms [59].

When the electrons of Ag_3PO_4 are excited from VB to CB, Ag_3PO_4 produces ROS and releases silver ions due to its gradual degradation [60]. These results corroborate with the data provided by the XRD, micro-Raman, and FE-SEM measurements, which show changes in

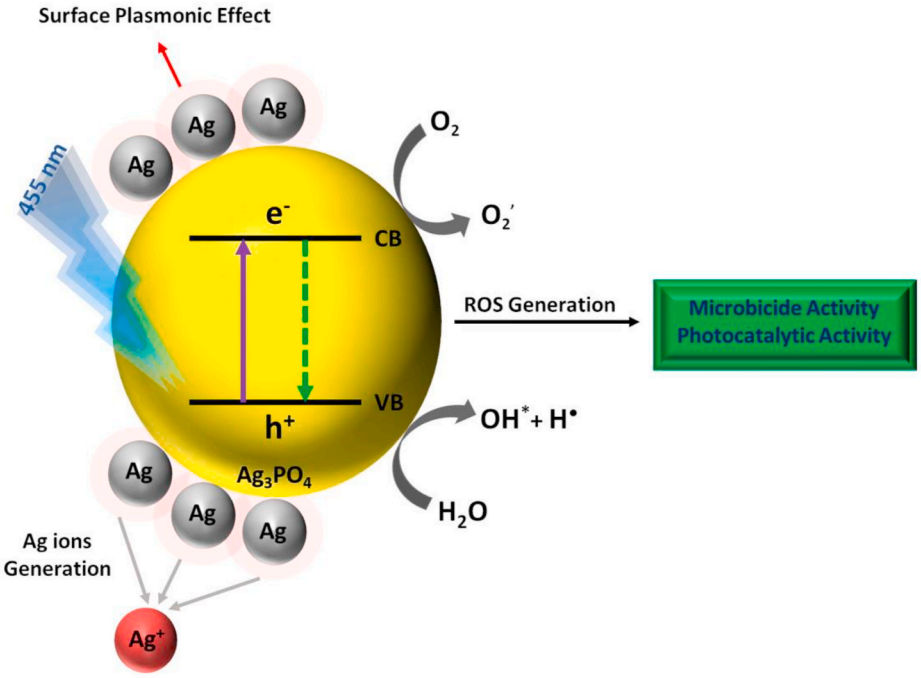

Fig. 8. A schematic representation of the mechanism for photodegradation and microbicide activity of synthesized Ag_3PO_4 microcrystals submitted to irradiation with visible-light (455 nm). SPE: surface plasmonic effect; e^-: electron; h^+: hole; CB: conduction band; VB: valence band.

Ag_3PO_4 at long and short ranges. The structural degradation of Ag_3PO_4 for the formation of metallic Ag was directly proportional to the morphological alteration of the material. Thus, it is suggested that a certain degree of disorder, both structural and morphological, is desirable for greater system efficiency.

3. Experimental

3.1. Synthesis

Ag_3PO_4 microcrystals were synthesized at room temperature by the CP method because it is a simple, low cost and fast method that does not require heat treatments, besides being widely used in the literature [61–63]. For that, 3×10^{-3} mol of silver nitrate ($AgNO_3$, Cennabras, 98%) and 1×10^{-3} mol of diammonium hydrogen phosphate ($[NH_4]_2HPO_4$, Alfa-Aesar, 98%) were separately dissolved in beakers containing 75 and 25 mL of distilled water, respectively. After complete dissolution, the precursors were mixed for 10 min under magnetic stirring, promoting the instant precipitation of Ag_3PO_4. The resulting precipitate was washed several times with distilled water and acetone to remove remaining ions in contact with the material. Subsequently, the obtained Ag_3PO_4 was centrifuged and oven dried at 60 °C.

3.2. Characterization

The Ag_3PO_4 microcrystals were characterized by XRD using a Rigaku D/Max 2500 PC (Japan) diffractometer. A scanning angle of 10 to 85°, scanning speed of 1°/min, angular pitch of 0.02°, and CuKα radiation (λ = 1.5406 Å) were used. To determine the band gap, a Varian Cary 5G spectrometer was used at a wavelength of 200 to 800 nm and scanning speed of 600 nm/min, using the Kubelka-Munk function [64,65]. The photocatalytic activity was evaluated considering the degradation of rhodamine B (RhB) in an aqueous solution under visible-light irradiation [1]. Thus, 50 mg of Ag3PO4 powder was mixed in 50 mL of 1 × 10-5 mol/L RhB solution for 15 min in an ultrasonic bath (1510 Branson, 42 kHz). The system was magnetically stirred in the dark for 30 min at 20 °C to promote adsorption-desorption between the dye and the powder. The temperature was controlled by a thermostatic bath. When the first aliquot of 2 mL was collected, the time was denominated as 0 min. Subsequently, there was an optical system, called "biotable", composed of 24 LEDs with 455-nm wavelength and 31 mW/cm^2 irradiance power in the suspension. In this system, aliquots were collected at different times: 0 (control, without the presence of Ag3PO4), 1 (1.86 J/cm^2), 3 (5.58 J/cm^2), 6 (11.16 J/cm^2), 9 (16.74 J/cm^2), 12 (22.32 J/cm^2), 15 (27.9 J/cm^2), 20 (37.2 J/cm^2), 25 (46.5 J/cm^2), and 30 (55.8 J/cm^2) minutes. The aliquots were centrifuged (MiniSpin) for 3 min (8300 rpm) and analyzed in the UV–Vis spectrophotometer to monitor the maximum absorption band of RhB (λ = 554 nm). To analyze the order/disorder of the system at short-range and the morphology and size of the samples, micro-Raman spectroscopy and FE-SEM (Carl Zeiss Microscope operated at 30 kV) were performed, respectively.

In order to propose a mechanism for the photocatalytic and fungicide activity of Ag_3PO_4, reactive species trapping test was performed as described previously [41,66]. Benzoquinone (BQ), ammonium oxalate (AO) and isopropanol (ISO) as scavengers for superoxide radical ($\cdot O_2^-$), holes (h^+) and hydroxyl radical ($\cdot OH$), respectively.

3.3. Antifungal tests using synthesized Ag_3PO_4

The synthesized Ag_3PO_4 microcrystals were tested to verify their antifungal ability against a standard strain of *C. albicans* from the American Type Culture Collection (ATCC) 90028. The test determined their MFC and MBIC [67] in both, planktonic and biofilms cells, in the presence and absence of light.

The frozen microorganisms were reactivated in a Sabouraud Dextrose Agar (SDA - Michigan, USA) culture medium with 5 μg/mL chloramphenicol, and incubated at 37 °C for 48 h. After this period, 5 colonies of similar size were transferred into 5 mL of Yeast Nitrogen Base (YNB - Maharashtra, India) specific culture medium in a Falcon tube, which was incubated at 37 °C for 16 h. Subsequently, 500 μL of pre-inoculum were diluted in 9.5 mL of YNB and incubated again for 8 h at 37 °C. The growth phase was determined by the optical density (OD 540 nm) of the suspension, which was standardized in a spectrophotometer at 0.55 (±0.08), with a concentration of approximately 7.94 ×

10^6 CFU/mL.

3.3.1. Microbiological tests in planktonic cells

After OD was reached, the growth rate was diluted (10^6 to 10^3). Subsequently, microcrystals diluted in 2 mL microtubes, with concentrations between 0.9 and 2000 μg/mL, were placed in 24-well plates (Kasvi–China). Samples of *C. albicans* at 10^3 were added to each well of the 24-well plates, for a total of 500 μL (250 μL of microcrystal and 250 μL of *C. albicans* suspension). Two plates were used: one exposed to visible-light (L+) and the other preserved in the dark (L-). Shortly after the contact between microorganisms and microcrystals, one plate was wrapped in aluminum foil and remained incubated at 37 °C for 30 min. The other plate was exposed to light at a 455-nm wavelength (55.8 J/cm^2) for the same period. After that, both plates were plated in duplicate by the drip method (10 μL) in Petri dishes containing SDA culture medium with chloramphenicol. The dishes were maintained in a static incubator at 37 °C for 24 h for subsequent counting of colony forming units (CFU/mL). The analyses were performed in triplicate and on three different occasions.

3.3.2. Microbiological tests of biofilms in formation

After OD was reached, *C. albicans* was added to two 24-well plates (TPP–Trasadingen, Switzerland) at a concentration of 10^7 (2 mL). The plates were placed in an orbital shaker (37 °C, 75 rpm) for 90 min to provide initial adhesion [68]. Subsequently, each well was washed two times with phosphate-buffered saline (PBS, 1 mL) to remove the weakly adhered microorganisms. After that, the wells were resuspended with 1 mL of YNB medium and 1 mL of microcrystals diluted in PBS, for a total of 2 mL with different concentrations in each well [69]. One plate was wrapped in aluminum foil and remained in the orbital shaker at 37 °C, while the other was exposed to visible-light at a 455-nm wavelength for 30 min. A blue (455 nm) light-emitting diode was chosen due to its great use in photoinactivation of oral microorganisms like *C. albicans* [70,71]. Next, the plate exposed to light was also wrapped in aluminum foil, and both plates remained in the orbital shaker at 37 °C for 48 h. Subsequently, both plates were removed from the orbital shaker, washed with 1 mL of PBS (three times), and resuspended in 2 mL of YNB. To count the colony forming units (CFU/mL), the biofilms were removed from the bottom of the plate with the aid of a sterile tip, and 20 μL aliquots of the detached biofilms were serially diluted in PBS (10^{-1} to 10^{-4}). Afterwards, 10 μL aliquots of each dilution (10^0 to 10^{-4}) were seeded in dishes containing SDA by the drip method (10 μL). The sowing procedures were performed in duplicate. Then, the Petri dishes were incubated for 24 h at 37 °C for subsequent counting of the colony forming units (CFU/mL). The LED device used, covered the wavelength range from 440 to 460 nm, with maximum emission at 455 nm and the analyses were performed in triplicate and on three different occasions.

3.3.3. Microscopy analyses of biofilm with microcrystals

The biofilm was formed in two 24-well plates (n = 2), and the growth protocol was followed as described above, resulting in a concentration of approximately 1×10^7 CFU/mL. After a 48h incubation, the particles were washed (three times), and the biofilm was marked with the fluorophores SYTO 9 and propidium iodide, which were present in the LIVE/DEAD kit and handled according to the manufacturer's instructions. The biofilms were maintained in PBS for visualization on the confocal fluorescence microscope (Carl Zeiss LSM 780, Thuringia, Germany) with 488 nm (excitation) and 561 nm (emission) lasers on the 20x objective. The images were analyzed in the ZEN Blue software version 2.3 (Thuringia, Germany) and this experiment was performed in triplicate in two independent occasions.

To analyze the morphology of the biofilm and microcrystals, FE-SEM (Thuringia, Germany) was used. For the biofilm analysis, polystyrene discs were cut from the bottom of a 24-well plate (Trasadingen, Switzerland). The discs were used with the biofilm during its growth in the bottom of the plate, following the same growth conditions described above, and using a concentration of approximately 1×10^7 CFU/mL. To sterilize the discs, they were added to a beaker containing 200 mL of distilled water and placed in a 645-W microwave for 3 min [72].

After 48 h of incubation, each well was washed with PBS (three times), and the disks that remained in the bottom throughout the biofilm growth were immersed for 20 min in paraformaldehyde and serially dehydrated in ethanol (70%, 80%, 90%, and 100%) for 20 min at each concentration. The disks were dried at room temperature and kept in a vacuum desiccator until the analysis, for which the field emission scanning electron microscope (Thuringia, Germany) was used. The obtained images used magnifications of 500x and 2500x at 10 kV and wavelength dispersion (WDS) of 8 mm. Before microscopic observation, the samples were mounted on metallic stubs and covered with gold.

3.4. Statistical analysis

In the present study, the concentration and the presence or absence of light were considered to be a variation factor. After verifying the normality and homogeneity of data, ANOVA two-way test was applied followed by posthoc Tukey ($\alpha = 0.05$) was performed. The statistical analysis was carried out using the software SPSS (IBM, NY, USA).

4. Conclusions

The main conclusions of the present work can be summarized as follows: (i) Ag_3PO_4 microcrystals were synthesized by the CP method, and after four cycles of light exposure at a 455-nm wavelength, cubic (from 1 exposure) and hexagonal Ag (from 3 exposures) were formed; (ii) after each exposure to light, it was observed that the [AgO_4] clusters, as building blocks of the 3D structure of Ag_3PO_4, are the sites where the formation of metallic Ag^0 takes place. This process favors material decomposition by altering its morphology at the end of the fourth light exposition, (iii) in the microbiological tests with and without light, Ag_3PO_4 presented antifungal activity for both planktonic and biofilm forms. However, it was observed that its antifungal activity was more effective with lower concentrations in the presence of light when compared to higher microcrystal concentrations in the absence of light; (iv) the antifungal activity of Ag_3PO_4 was increased by visible-light irradiation; and (v) based on the present results related to antimicrobial capacity, durability and long-term use, we believe this study is of fundamental importance to the design of photocatalytic and fungicide Ag_3PO_4 based materials.

Declaration of competing interest

The authors declare that they have no known competing financial interests or personal relationships that could have appeared to influence the work reported in this paper.

Acknowledgments

The authors are grateful to São Paulo Research Foundation – FAPESP (grant # CDMF: 2013/07296-2; Bruna Natália Alves da Silva Pimentel was supported by FAPESP grant #2015/13834-2; Camila Cristina de Foggi was supported by FAPESP grant #2017/12594-3 and #2019/13507-2), and CAPES (Coordination for the Improvement of Higher Education Personnel - Finance Code 001), for financially supporting this research. JA acknowledges financial support from Universitat Jaume I, for project UJI-B2019-30, and Ministerio de Ciencia, Innovación y Universidades (Spain) project PGC2018-094417-B-I00.

Appendix A. Supplementary data

Supplementary data to this article can be found online at https://doi.org/10.1016/j.ceramint.2021.04.272.

References

[1] G. Botelho, J. Andres, L. Gracia, L.S. Matos, E. Longo, Photoluminescence and photocatalytic properties of Ag3PO4 microcrystals: an experimental and theoretical investigation, Chempluschem 81 (2016) 202–212, https://doi.org/10.1002/cplu.201500485.

[2] F. Teng, Z. Liu, A. Zhang, M. Li, Photocatalytic performances of Ag3PO4 polypods for degradation of dye pollutant under natural indoor weak light irradiation, Environ. Sci. Technol. 49 (2015) 9489–9494, https://doi.org/10.1021/acs.est.5b00735.

[3] Z. Yi, J. Ye, N. Kikugawa, T. Kako, S. Ouyang, H. Stuart-Williams, H. Yang, J. Cao, W. Luo, Z. Li, Y. Liu, R.L. Withers, An orthophosphate semiconductor with photooxidation properties under visible-light irradiation, Nat. Mater. 9 (2010) 559, https://doi.org/10.1038/nmat2780.

[4] Y. Bi, S. Ouyang, N. Umezawa, J. Cao, J. Ye, Facet effect of single-crystalline Ag3PO4 sub-microcrystals on photocatalytic properties, J. Am. Chem. Soc. 133 (2011) 6490–6492, https://doi.org/10.1021/ja2002132.

[5] N. Lu, P. Zhang, Q. Zhang, R. Qiao, Q. He, H.-B. Li, Y. Wang, J. Guo, D. Zhang, Z. Duan, Z. Li, M. Wang, S. Yang, M. Yan, E. Arenholz, S. Zhou, W. Yang, L. Gu, C.-W. Nan, J. Wu, Y. Tokura, P. Yu, Electric-field control of tri-state phase transformation with a selective dual-ion switch, Nature 546 (2017) 124–128, https://doi.org/10.1038/nature22389.

[6] X. Chen, Y. Dai, X. Wang, Methods and mechanism for improvement of photocatalytic activity and stability of Ag3PO4: a review, J. Alloys Compd. 649 (2015) 910–932, https://doi.org/10.1016/j.jallcom.2015.07.174.

[7] X. Shi, H. Chen, F. Hao, R. Liu, T. Wang, P. Qiu, U. Burkhardt, Y. Grin, L. Chen, Room-temperature ductile inorganic semiconductor, Nat. Mater. 17 (2018) 421–426, https://doi.org/10.1038/s41563-018-0047-z.

[8] J.F. Cruz-Filho, T.M.S. Costa, M.S. Lima, L.J. Silva, R.S. Santos, L.S. Cavalcante, E. Longo, G.E. Luz, Effect of different synthesis methods on the morphology, optical behavior, and superior photocatalytic performances of Ag3PO4 sub-microcrystals using white-light-emitting diodes, J. Photochem. Photobiol. A Chem. 377 (2019) 14–25, https://doi.org/10.1016/j.jphotochem.2019.03.031.

[9] F. Lipsky, L.H. da S. Lacerda, S.R. de Lazaro, E. Longo, J. Andrés, M.A. San-Miguel, Unraveling the relationship between exposed surfaces and the photocatalytic activity of Ag3PO4: an in-depth theoretical investigation, RSC Adv. 10 (2020) 30640–30649, https://doi.org/10.1039/D0RA06045C.

[10] M. Al Kausor, S. Sen Gupta, D. Chakrabortty, Ag3PO4-based nanocomposites and their applications in photodegradation of toxic organic dye contaminated wastewater: review on material design to performance enhancement, J. Saudi Chem. Soc. 24 (2020) 20–41, https://doi.org/10.1016/j.jscs.2019.09.001.

[11] D.J. Martin, G. Liu, S.J.A. Moniz, Y. Bi, A.M. Beale, J. Ye, J. Tang, Efficient visible driven photocatalyst, silver phosphate: performance, understanding and perspective, Chem. Soc. Rev. 44 (2015) 7808–7828, https://doi.org/10.1039/C5CS00380F.

[12] A. Pavanello, A. Blasco, P.F. Johnston, M.A. Miranda, M.L. Marin, Enhanced photodegradation of synthetic dyes mediated by Ag3PO4-based semiconductors under visible light irradiation, Catalysts 10 (2020) 774.

[13] U. Chilakamarthi, L. Giribabu, Photodynamic therapy: past, present and future, Chem. Rec. 17 (2017) 775–802, https://doi.org/10.1002/tcr.201600121.

[14] L. Zeng, Y. Pan, Y. Tian, X. Wang, W. Ren, S. Wang, G. Lu, A. Wu, Doxorubicin-loaded NaYF4:Yb/Tm–TiO2 inorganic photosensitizers for NIR-triggered photodynamic therapy and enhanced chemotherapy in drug-resistant breast cancers, Biomaterials 57 (2015) 93–106, https://doi.org/10.1016/j.biomaterials.2015.04.006.

[15] D.P. Lynch, Oral candidiasis: history, classification, and clinical presentation, Oral Surgery, Oral Med. Oral Pathol. 78 (1994) 189–193, https://doi.org/10.1016/0030-4220(94)90146-5.

[16] J.W. Millsop, N. Fazel, Oral candidiasis, Clin. Dermatol. 34 (2016) 487–494, https://doi.org/10.1016/j.clindermatol.2016.02.022.

[17] L. Gendreau, Z.G. Loewy, Epidemiology and etiology of denture stomatitis, J. Prosthodont. 20 (2011) 251–260, https://doi.org/10.1111/j.1532-849X.2011.00698.x.

[18] L.N. Dovigo, A.C. Pavarina, A.P.D. Ribeiro, I.L. Brunetti, C.A. de S. Costa, D. P. Jacomassi, V.S. Bagnato, C. Kurachi, Investigation of the photodynamic effects of curcumin against Candida albicans, Photochem. Photobiol. 87 (2011) 895–903, https://doi.org/10.1111/j.1751-1097.2011.00937.x.

[19] L.-W. Zhang, J.-Y. Fu, H. Hua, Z.-M. Yan, Efficacy and safety of miconazole for oral candidiasis: a systematic review and meta-analysis, Oral Dis. 22 (2016) 185–195, https://doi.org/10.1111/odi.12380.

[20] S. Antinori, L. Milazzo, S. Sollima, M. Galli, M. Corbellino, Candidemia and invasive candidiasis in adults: a narrative review, Eur. J. Intern. Med. 34 (2016) 21–28, https://doi.org/10.1016/j.ejim.2016.06.029.

[21] B.N.A. da S. Pimentel, C.C. de Foggi, P.A. Barbugli, R.C. de Oliveira, E.D. de Avila, E. Longo, C.E. Vergani, Antifungal activity and biocompatibility of α-AgVO3 microcrystals: a promising material against oral Candida disease, Mater. Sci. Eng. C 108 (2020) 110405, https://doi.org/10.1016/j.msec.2019.110405.

[22] C.C. De Foggi, R.C. De Oliveira, M. Assis, M.T. Fabbro, V.R. Mastelaro, C. E. Vergani, L. Gracia, J. Andrés, E. Longo, A.L. Machado, Unveiling the role of β-Ag2MoO4 microcrystals to the improvement of antibacterial activity, Mater. Sci. Eng. C 111 (2020) 110765.

[23] I.M. Pinatti, A.C.M. Tello, A.B. Trench, C.C. de Foggi, P.F.S. Pereira, M.M. Teixeira, N. Jacomaci, J. Andrés, E. Longo, Zinc-substituted Ag2CrO4: a material with enhanced photocatalytic and biological activity, J. Alloys Compd. 835 (2020) 155315, https://doi.org/10.1016/j.jallcom.2020.155315.

[24] R.C. de Oliveira, C.C. de Foggi, M.M. Teixeira, M.D.P. da Silva, M. Assis, E. M. Francisco, B.N.A. da S. Pimentel, P.F. dos, S. Pereira, C.E. Vergani, A. L. Machado, J. Andres, L. Gracia, E. Longo, Mechanism of antibacterial activity via morphology change of α-AgVO3: theoretical and experimental insights, ACS Appl. Mater. Interfaces 9 (2017) 11472–11481, https://doi.org/10.1021/acsami.7b00920.

[25] A.B. Trench, T.R. Machado, A.F. Gouveia, C.C. Foggi, V. Teodoro, I. Sánchez-Montez, M.M. Teixeira, L.G. da Trindade, N. Jacomaci, A. Perrin, C. Perrin, J. M. Aquino, J. Andrés, E. Longo, Rational design of W-doped Ag3PO4 as an efficient antibacterial agent and photocatalyst for organic pollutant degradation, ACS Omega 5 (37) (2020) 23808–23821, https://doi.org/10.1021/acsomega.0c03019.

[26] C.C. Foggi, M.T. Fabbro, L.P.S. Santos, Y.V.B. de Santana, C.E. Vergani, A. L. Machado, E. Cordoncillo, J. Andrés, E. Longo, Synthesis and evaluation of α-Ag2WO4 as novel antifungal agent, Chem. Phys. Lett. 674 (2017) 125–129, https://doi.org/10.1016/j.cplett.2017.02.067.

[27] C.C. de Foggi, R.C. de Oliveira, M.T. Fabbro, C.E. Vergani, J. Andres, E. Longo, A. L. Machado, Tuning the morphological, optical, and antimicrobial properties of α-Ag2WO4 microcrystals using different solvents, Cryst. Growth Des. 17 (2017) 6239–6246, https://doi.org/10.1021/acs.cgd.7b00786.

[28] N.L.H. Chávez, E.D. de Avila, P.A. Barbugli, R.C. de Oliveira, C.C. de Foggi, E. Longo, C.E. Vergani, Promising effects of silver tungstate microcrystals on fibroblast human cells and three dimensional collagen matrix models: a novel non-cytotoxic material to fight oral disease, Colloids Surf. B Biointerfaces 170 (2018) 505–513.

[29] M. Assis, T. Robeldo, C.C. Foggi, A.M. Kubo, G. Mínguez-Vega, E. Condoncillo, H. Beltran-Mir, R. Torres-Mendieta, J. Andrés, M. Oliva, C.E. Vergani, P. A. Barbugli, E.R. Camargo, R.C. Borra, E. Longo, Ag nanoparticles/α-Ag2WO4 composite formed by electron beam and femtosecond irradiation as potent antifungal and antitumor agents, Sci. Rep. 9 (2019) 9927, https://doi.org/10.1038/s41598-019-46159-y.

[30] M. Ohara, Y. Kawashima, S. Kitajima, C. Mitsuoka, H. Watanabe, Blue light inhibits the growth of skin tumors in the v-Ha-ras transgenic mouse, Canc. Sci. 94 (2003) 205–209, https://doi.org/10.1111/j.1349-7006.2003.tb01420.x.

[31] P.-S. Oh, K.S. Na, H. Hwang, H.-S. Jeong, S. Lim, M.-H. Sohn, H.-J. Jeong, Effect of blue light emitting diodes on melanoma cells: involvement of apoptotic signaling, J. Photochem. Photobiol. B Biol. 142 (2015) 197–203, https://doi.org/10.1016/j.jphotobiol.2014.12.006.

[32] Y. Yuan, G. Yan, R. Gong, L. Zhang, T. Liu, C. Feng, W. Du, Y. Wang, F. Yang, Y. Li, S. Guo, F. Ding, W. Ma, E. Idiiatullina, V. Pavlov, Z. Han, B. Cai, L. Yang, Effects of blue light emitting diode irradiation on the proliferation, apoptosis and differentiation of bone marrow-derived mesenchymal stem cells, Cell. Physiol. Biochem. 43 (2017) 237–246, https://doi.org/10.1159/000480344.

[33] K. Wang, D. Yang, M. Xiao, X. Chen, F. Lu, J. Nie, Sesamin as a co-initiator for unfilled dental restorations, Acta Biomater. 5 (2009) 2508–2517, https://doi.org/10.1016/j.actbio.2009.03.008.

[34] H.-J. Moon, D.-H. Shin, Effect of CQ-amine ratio on the degree of conversion in resin monomers with binary and ternary photoinitiation systems, Rde 37 (2012) 96–102, https://doi.org/10.5395/rde.2012.37.2.96.

[35] D.G. Pitts, T.J. Tredici, The effects of ultraviolet on the eye, Am. Ind. Hyg. Assoc. J. 32 (1971) 235–246, https://doi.org/10.1080/0002889718506444.

[36] W.L. Epstein, K. Fukuyama, J.H. Epstein, Early effects of ultraviolet light on DNA synthesis in human skin in vivo, Arch. Dermatol. 100 (1969) 84–89, https://doi.org/10.1001/archderm.1969.01610250090021.

[37] H.R. Griffiths, P. Mistry, K.E. Herbert, J. Lunec, Molecular and cellular effects of ultraviolet light-induced genotoxicity, Crit. Rev. Clin. Lab Sci. 35 (1998) 189–237, https://doi.org/10.1080/10408369891234192.

[38] R. Nomoto, Effect of light wavelength on polymerization of light-cured resins, Dent. Mater. J. 16 (1997) 60–73.

[39] P.F.S. Pereira, A.F. Gouveia, M. Assis, R.C. de Oliveira, I.M. Pinatti, M. Penha, R. F. Gonçalves, L. Gracia, J. Andrés, E. Longo, ZnWO4 nanocrystals: synthesis, morphology, photoluminescence and photocatalytic properties, Phys. Chem. Chem. Phys. 20 (2018) 1923–1937, https://doi.org/10.1039/C7CP07354B.

[40] B. Liu, X. Zhao, C. Terashima, A. Fujishima, K. Nakata, Thermodynamic and kinetic analysis of heterogeneous photocatalysis for semiconductor systems, Phys. Chem. Chem. Phys. 16 (2014) 8751–8760, https://doi.org/10.1039/C3CP55317E.

[41] M. Ge, Photodegradation of rhodamine B and methyl orange by Ag3PO4 catalyst under visible light irradiation, Chin. J. Catal. 35 (2014) 1410–1417.

[42] X.-Z. Li, K.-L. Wu, C. Dong, S.-H. Xia, Y. Ye, X.-W. Wei, Size-controlled synthesis of Ag3PO4 nanorods and their high-performance photocatalysis for dye degradation under visible-light irradiation, Mater. Lett. 130 (2014) 97–100, https://doi.org/10.1016/j.matlet.2014.05.069.

[43] K.V. Kumar, K. Porkodi, F. Rocha, Langmuir–Hinshelwood kinetics – a theoretical study, Catal. Commun. 9 (2008) 82–84, https://doi.org/10.1016/j.catcom.2007.05.019.

[44] G. Botelho, J.C. Sczancoski, J. Andres, L. Gracia, E. Longo, Experimental and theoretical study on the structure, optical properties, and growth of metallic silver nanostructures in Ag3PO4, J. Phys. Chem. C 119 (2015) 6293–6306, https://doi.org/10.1021/jp512111v.

[45] F. Rahmawati, S. Wahyuningsih, D. Irianti, The photocatalytic activity of SiO 2-TiO 2/graphite and its composite with silver and silver oxide, Bull. Chem. React. Eng. Catal. 9 (2014).

[46] F. Rahmawati, T. Kusumaningsih, A.M. Hapsari, A. Hastuti, Ag and Cu loaded on TiO2/graphite as a catalyst for Escherichia coli-contaminated water disinfection, Chem. Pap. 64 (2010) 557–565, https://doi.org/10.2478/s11696-010-0036-4.

[47] P. Taneja, R. Banerjee, P. Ayyub, G.K. Dey, Observation of a hexagonal $(4H)$ phase in nanocrystalline silver, Phys. Rev. B 64 (2001) 33405, https://doi.org/10.1103/PhysRevB.64.033405.
[48] I. Chakraborty, S.N. Shirodkar, S. Gohil, U.V. Waghmare, P. Ayyub, The nature of the structural phase transition from the hexagonal (4H) phase to the cubic (3C) phase of silver, J. Phys. Condens. Matter 26 (2014) 115405, https://doi.org/10.1088/0953-8984/26/11/115405.
[49] V.M. Longo, C.C. De Foggi, M.M. Ferrer, A.F. Gouveia, R.S. André, W. Avansi, C. E. Vergani, A.L. Machado, J. Andrés, L.S. Cavalcante, A.C. Hernandes, E. Longo, Potentiated electron transference in α-Ag2WO4 microcrystals with Ag nanofilaments as microbial agent, J. Phys. Chem. A 118 (2014) 5769–5778, https://doi.org/10.1021/jp410564p.
[50] C.G. Pierce, T. Vila, J.A. Romo, D. Montelongo-Jauregui, G. Wall, A. Ramasubramanian, J.L. Lopez-Ribot, The Candida albicans biofilm matrix: composition, structure and function, J. Fungi 3 (2017) 14.
[51] S. Kucharíková, H. Tournu, K. Lagrou, P. Van Dijck, H. Bujdakova, Detailed comparison of Candida albicans and Candida glabrata biofilms under different conditions and their susceptibility to caspofungin and anidulafungin, J. Med. Microbiol. 60 (2011) 1261–1269.
[52] S. Chernousova, M. Epple, Silver as antibacterial agent: ion, nanoparticle, and metal, Angew. Chem. Int. Ed. 52 (2013) 1636–1653.
[53] J.R. Morones, J.L. Elechiguerra, A. Camacho, K. Holt, J.B. Kouri, J.T. Ramírez, M. J. Yacaman, The bactericidal effect of silver nanoparticles, Nanotechnology 16 (2005) 2346.
[54] L.N. Dovigo, A.C. Pavarina, E.G. de Oliveira Mima, E.T. Giampaolo, C.E. Vergani, V.S. Bagnato, Fungicidal effect of photodynamic therapy against fluconazole-resistant Candida albicans and Candida glabrata, Mycoses 54 (2011) 123–130.
[55] C. So, P.W.K. Tsang, P. Lo, C.J. Seneviratne, L.P. Samaranayake, W. Fong, Photodynamic inactivation of Candida albicans by BAM-SiPc, Mycoses 53 (2010) 215–220.
[56] S. Thiyagarajan, S. Singh, D. Bahadur, Reusable sunlight activated photocatalyst Ag3PO4 and its significant antibacterial activity, Mater. Chem. Phys. 173 (2016) 385–394.
[57] S. Prabhu, E.K. Poulose, Silver nanoparticles: mechanism of antimicrobial action, synthesis, medical applications, and toxicity effects, Int. Nano Lett. 2 (2012) 32.
[58] J.-K. Liu, C.-X. Luo, J.-D. Wang, X.-H. Yang, X.-H. Zhong, Controlled synthesis of silver phosphate crystals with high photocatalytic activity and bacteriostatic activity, CrystEngComm 14 (2012) 8714–8721, https://doi.org/10.1039/C2CE25604E.
[59] C.J. Nobile, A.D. Johnson, Candida albicans biofilms and human disease, Annu. Rev. Microbiol. 69 (2015) 71–92.
[60] N.K. Eswar, P.C. Ramamurthy, G. Madras, Enhanced sunlight photocatalytic activity of Ag 3 PO 4 decorated novel combustion synthesis derived TiO 2 nanobelts for dye and bacterial degradation, Photochem. Photobiol. Sci. 14 (2015) 1227–1237.
[61] J. Zhang, H. Bi, G. He, Y. Zhou, H. Chen, Fabrication of Ag3PO4− PANI− GO composites with high visible light photocatalytic performance and stability, J. Environ. Chem. Eng. 2 (2014) 952–957.
[62] P. Amornpitoksuk, S. Suwanboon, Comparative study of the photocatalytic decolorization of rhodamine B dye by AgI-Ag3PO4 prepared from co-precipitation and ion-exchange methods, J. Alloys Compd. 720 (2017) 582–588.
[63] R. Liu, P. Hu, S. Chen, Photocatalytic activity of Ag3PO4 nanoparticle/TiO2 nanobelt heterostructures, Appl. Surf. Sci. 258 (2012) 9805–9809.
[64] M. Nowak, B. Kauch, P. Szperlich, Determination of energy band gap of nanocrystalline SbSI using diffuse reflectance spectroscopy, Rev. Sci. Instrum. 80 (2009) 46107.
[65] B. Philips-Invernizzi, D. Dupont, C. Caze, Bibliographical review for reflectance of diffusing media, Opt. Eng. 40 (2001) 1082–1092.
[66] A.B. Trench, T.R. Machado, A.F. Gouveia, M. Assis, L.G. da Trindade, C. Santos, A. Perrin, C. Perrin, M. Oliva, J. Andrés, E. Longo, Connecting structural, optical, and electronic properties and photocatalytic activity of Ag3PO4:Mo complemented by DFT calculations, Appl. Catal. B Environ. 238 (2018) 198–211, https://doi.org/10.1016/j.apcatb.2018.07.019.
[67] P. Van Dijck, J. Sjollema, B.P.A. Cammue, K. Lagrou, J. Berman, C. d'Enfert, D. R. Andes, M.C. Arendrup, A.A. Brakhage, R. Calderone, Methodologies for in vitro and in vivo evaluation of efficacy of antifungal and antibiofilm agents and surface coatings against fungal biofilms, Microb. Cell. 5 (2018) 300.
[68] J. Chandra, P.K. Mukherjee, S.D. Leidich, F.F. Faddoul, L.L. Hoyer, L.J. Douglas, M. A. Ghannoum, Antifungal resistance of candidal biofilms formed on denture acrylic in vitro, J. Dent. Res. 80 (2001) 903–908, https://doi.org/10.1177/00220345010800031101.
[69] F. Martinez-Gutierrez, P.L. Olive, A. Banuelos, E. Orrantia, N. Nino, E.M. Sanchez, F. Ruiz, H. Bach, Y. Av-Gay, Synthesis, characterization, and evaluation of antimicrobial and cytotoxic effect of silver and titanium nanoparticles, Nanomed. Nanotechnol. Biol. Med. 6 (2010) 681–688.
[70] E.G. de O. Mima, A.C. Pavarina, L.N. Dovigo, C.E. Vergani, C.A. de S. Costa, C. Kurachi, V.S. Bagnato, Susceptibility of Candida albicans to photodynamic therapy in a murine model of oral candidosis, Oral Surgery, Oral Med. Oral Pathol. Oral Radiol. Endodontol. 109 (2010) 392–401, https://doi.org/10.1016/j.tripleo.2009.10.006.
[71] M.C. Andrade, A.P.D. Ribeiro, L.N. Dovigo, I.L. Brunetti, E.T. Giampaolo, V. S. Bagnato, A.C. Pavarina, Effect of different pre-irradiation times on curcumin-mediated photodynamic therapy against planktonic cultures and biofilms of Candida spp, Arch. Oral Biol. 58 (2013) 200–210, https://doi.org/10.1016/j.archoralbio.2012.10.011.
[72] M.M. Silva, E.G. de O. Mima, A.L. Colombo, P.V. Sanitá, J.H. Jorge, E.M. S. Massucato, C.E. Vergani, Comparison of denture microwave disinfection and conventional antifungal therapy in the treatment of denture stomatitis: a randomized clinical study, Oral Surg, Oral Med. Oral Pathol. Oral Radiol. 114 (2012) 469–479, https://doi.org/10.1016/j.oooo.2012.05.006.